



PCCP

Relatives of Cyanomethylene: Replacement of the Divalent Carbon by B⁻, N⁺, Al⁻, Si, P⁺, Ga⁻, Ge, As⁺

Journal:	<i>Physical Chemistry Chemical Physics</i>
Manuscript ID	CP-ART-10-2019-005777.R1
Article Type:	Paper
Date Submitted by the Author:	13-Nov-2019
Complete List of Authors:	Abbott, Boyi; University of Georgia , Center for Computational Chemistry Hoobler, Preston; Covenant College, Chemistry; University of Georgia Franklin College of Arts and Sciences, Center for Computational Quantum Chemistry Schaefer, Henry; University of Georgia, Computational Chemistry

SCHOLARONE™
Manuscripts

Cite this: DOI: 00.0000/xxxxxxxxxx

Relatives of Cyanomethylene: Replacement of the Divalent Carbon by B⁻, N⁺, Al⁻, Si, P⁺, Ga⁻, Ge, and As⁺

Boyi Z. Abbott,^{*a} Preston R. Hoobler,^a and Henry F. Schaefer III^{* a}Received Date
Accepted Date

DOI: 00.0000/xxxxxxxxxx

The lowest lying singlet and triplet states of HBCN⁻, HCCN, HNCN⁺, HAICN⁻, HSiCN, HPCN⁺, HGaCN⁻, HGeCN, and HAsCN⁺ were studied using the CCSDT(Q)/CBS//CCSD(T)/ aug-cc-pVQZ level of theory. Periodic trends in geometries, singlet-triplet gaps, and barriers to linearity were established and analyzed. The first row increasingly favors the triplet state, with a singlet-triplet gap ($\Delta E_{ST} = E_{\text{singlet}} - E_{\text{triplet}}$) of 3.5 kcal mol⁻¹, 11.9 kcal mol⁻¹, and 22.6 kcal mol⁻¹, respectively, for HBCN⁻, HCCN, and HNCN⁺. The second row increasing favors the singlet state, with singlet-triplet gaps of -20.4 kcal mol⁻¹ (HAICN⁻), -26.6 kcal mol⁻¹ (HSiCN), and -26.8 kcal mol⁻¹ (HPCN⁺). The third row also favors the singlet state, with singlet-triplet gaps of -26.8 kcal mol⁻¹ (HGaCN⁻), -33.5 kcal mol⁻¹ (HGeCN), and -33.1 kcal mol⁻¹ (HAsCN⁺). The HXCN species have larger absolute singlet-triplet energy gaps compared to their parent species XH₂ except for the case of X=N⁺. The effect of the substitution of hydrogen with a cyano group was analyzed with isodesmic bond separation analysis and NBO.

Introduction

Background

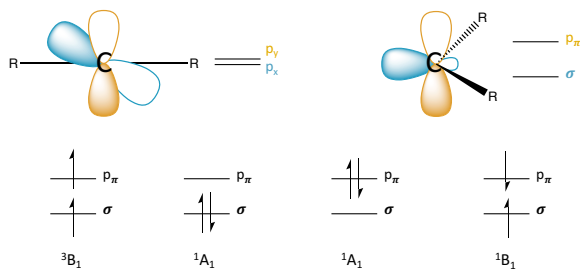


Fig. 1 Linear and bent geometries of carbenes and their electronic configurations.

It is well known that the spin states of carbenes dictate their reactivities.^{1–15} Carbenes with linear geometries possess two degenerate p orbitals (p_x , p_y). As the carbene bends, the p_x orbital becomes increasingly sp^2 -like in hybridization while the out-of-plane p_y retains its p -character (Figure 1), lifting the previous degeneracy. We will refer to the sp^2 -like orbital as σ and the out-of-plane p orbital as p_π . The two carbon-centered valence

electrons can either be spin-unpaired, leading to a triplet B_1 state (in the case of C_{2v} symmetry), or spin-paired, leading to singlet A_1 and B_1 states. The lowest-lying singlet state is typically the 1A_1 state with electron occupation in the σ orbital, whose energy is lowered as the geometry moves away from linearity. The ground state multiplicity of carbenes is qualitatively dependent on the energy separation between the σ and p_π orbitals, where a triplet ground state is more favorable if the separation is small. Equilibrium geometries of triplet states thus almost always have larger R–C–R (where C is the divalent carbon) angles than the corresponding singlet states.^{16–18}

Singlet carbenes have been utilized to achieve stereospecific one-step addition to carbon-carbon double bonds, as well as insertion into O–H bonds.^{5,6} Triplet carbenes, in contrast, undergo a non-stereospecific two-step addition to carbon double-bonds and participate in hydrogen abstraction reactions. Controlling the spin state of carbenes through various substituent and solvent substitutions has thus been a subject of study since the 1950s. Numerous recent reviews have been written summarizing both experimental^{8,10,11,13,14} and computational^{4,15} studies on the influence of substituents and solvents on the spin state of carbenes, and we refer the reader to these for a more comprehensive overview of carbene history.

Also of interest is the effect of substitution of the divalent carbon by other atoms. A natural choice of replacement would be with atoms in the same group, such as silicon (silylenes) and germanium (germylenes), and indeed there are many such studies.^{17–23} A different substitution involves the replacement of carbon with the isoelectronic nitrogen cation^{24,25} as well as others

^a Center for Computational Quantum Chemistry, University of Georgia, 140 Cedar Street, Athens, Georgia 30602, USA. Fax: +1 706 542-0406; Tel: +1 706 542-2067; E-mail: ccq@uga.edu

† Electronic Supplementary Information (ESI) available. See DOI: 10.1039/cXCP00000x/

in that group (P^+ , As^+). More recently, there has been increasing interest in group 13 anions such as B^- and Al^- as carbene substitutes.^{26–28} Few of these studies focus on comparing more than two different divalent atom species and instead focus on substituent effects on singlet-triplet (ST) gaps. The most comprehensive comparison of periodic trends for the substitution of the divalent atom comes from Cramer and coworkers,²⁹ who used density functional theory (DFT) and multi-reference methods to study the XH_2 species, $X = B^-, C, N^+, Al^-, Si, P^+, Ga^-, Ge, As^+$. The substituted valence-isoelectronic atoms form a three by three block on the periodic table, and gives an adequate representation of row and column effects.

In the present study, we look at the same nine valence-isoelectronic atoms of Cramer and coworkers, but with the cyano-substituted $HXCN$ species instead of XH_2 . Carbenes with cyano (CN) substituents are interesting not only due to their relevance in organic chemistry,³⁰ but because of their importance in combustion and atmospheric chemistry. Cyanomethylene (HCCN) is a major product of pyridine decomposition and a precursor of molecules found on Titan's atmosphere.^{31–34} Due to its relevance to atmospheric chemistry, its reaction with O_2 ^{34,35}, H ³⁶, CH_3 ³⁶, and NO ^{35,37} have all been investigated. Additionally, HCCN is thought to be an intermediate in HCN and HNC related reactions, which are important in interstellar chemistry^{38–45}, and has been identified as a candidate to forming acrylonitrile in the interstellar medium through a reaction with CH_2 .⁴⁶ Given the important applications of cyanocarbenes, it would be of interest to study how substitution of the divalent carbon with other atoms affects their electronic structures.

Previous work

Group 13.

Reactions of B, Al, and Ga atoms with HCN, in which $HXCN$ ($X = B, Al, Ga$) acts as an intermediate, have been subjects to a variety of combined experimental and theoretical studies. Andrews and coworkers have looked at reactions of B – Ti atoms with HCN in a solid argon matrix with accompanying DFT computations.^{47,48} Miller, Douberly and coworkers have analyzed the reactions of Al, Ga, and In with HCN via spectroscopy in helium nanodroplets accompanied with *ab initio* computations.^{49,50} However, these studies focused on the radical, not the anion that is isoelectronic with the cyanocarbene species. The only theoretical studies involving $HXCN$ ($X = B^-, Al^-, Ga^-$) is the 1996 work of Liebman and coworkers on the singlet and triplet states of $HBCN^-$ with MBPT2 geometries and coupled cluster single point energies.^{51,52}

Group 14.

The HCCN radical has long been the subject of experimental^{53–72} and computational^{33,59,73–90} study. Its interesting history has been characterized by disagreements regarding its triplet ground state geometry. Early experiments from the 1960s–1980s^{53–58} supported a linear equilibrium geometry while theory^{59,74–78,80,83} led by Kim, Schaefer, Pople, Radom, and coworkers consistently found that a bent equilibrium geometry is lower in energy. Since then, theory has been confirmed based on more

recent experimental studies. HCCN is a bent molecule, with an estimated barrier to linearity of between 240 and 300 cm^{-1} (0.67 and 0.86 $kcal\ mol^{-1}$).^{62,63,65–68,83,87}

Although silicon is also considered to be abundant in space^{91–94} and the cyanocarbene relative cyanosilylene (HSiCN) is thought to be detectable,^{95,96} there have been fewer studies on this molecule.^{64,95–102} In 1998, Maier and coworkers studied the reaction between Si and HCN in an argon matrix and observed HSiCN as an isomerization product.⁶⁴ HSiCN was detected by Thaddeus and coworkers in 2002 via microwave spectroscopy.⁹⁵ Flores and Carballera used DFT and multi-reference methods to study the lowest-lying singlet and triplet isomers of HSiCN.⁹⁷ Ding and coworkers have considered the potential energy surface of HSiCN and its isomers with DFT⁹⁸. Kalcher studied various cyanosilylenes with RHF-ACPF and CAS(2,2)-ACPF methods^{99,100}. Thorwirth and Harding have examined various isomers of singlet HSiCN with coupled cluster theory.¹⁰¹ Zhang and coworkers have looked at the low-lying excited states of HSiCN and HSiNC with CASSCF and CASPT2 methods.⁹⁶ Various experimental^{103–105} and computational^{106–108} studies exist on species containing germanium and cyano groups, but the only theoretical study on HGeCN known to us is by Kassae and coworkers (2005), who used various *ab initio* and DFT approaches to investigate the singlet and triplet states of HGeCN ($X = H, F, Cl, Br$).¹⁰⁹

Group 15.

Like HCCN, the HNCN radical is believed to be an important molecule in atmospheric chemistry.^{110–114} Its reaction with OH ¹¹⁰, NO ^{111,112}, and CN ¹¹³, as well as its role as an intermediate in the reaction $CH + N_2$ ¹¹⁴ have all been investigated theoretically. The HNCN cation, however, has significantly fewer studies. Puzzarini and Gambi performed a coupled-cluster study on the triplet state of $HNCN^+$ along with the parent HNCN radical and HNCN anion.¹¹⁵ Antoniotti and coworkers examined the singlet and triplet states of $HNCN^+$ and its isomers using multi-reference methods.¹¹⁶ Betterton studied singlet and triplet $HPCN^+$ and the HPCN radical using DFT.¹¹⁷ There has been no theoretical study on the $HAsCN^+$ molecule.

In this work, we use rigorous *ab initio* methods to study the lowest lying singlet and triplet states of $HBCN^-$, HCCN, $HNCN^+$, $HAICN^-$, HSiCN, $HPCN^+$, $HGaCN^-$, HGeCN, and $HAsCN^+$ to gauge periodic effects on structure and energetics. Periodic trends for geometry parameters, singlet-triplet (ST) gaps, and barriers to linearity will be discussed, and quantitative chemical analysis will be provided to understand these trends. In addition, we will compare the ST gaps of $HXCN$ with those of XH_2 and use isodesmic bond separation analysis and natural bond orbital analysis to decompose the differences in ST gaps between the two species. Throughout the study we will use “row one” to refer to $HXCN$ where $X = B^-, C, or N^+$, “row two” for $X = Al^-, Si, or P^+$, and “row three” for $X = Ga^-, Ge, or As^+$.

Methods

Geometries and Vibrational Frequencies

Geometry optimizations and harmonic frequencies were obtained for the lowest lying singlet and triplet states of the

nine cyanocarbene-like species using coupled cluster theory with singles, doubles, and perturbative triples excitations [CCSD(T)]^{118–120}. The $1s$ electrons of boron, carbon, and nitrogen were not correlated; the $1s$, $2s$, and $2p$ electrons of aluminum, silicon, and phosphorus were not correlated; and the $1s$, $2s$, $2p$, $3s$, and $3p$ electrons of gallium, germanium, and arsenic were not correlated. These frozen core settings were used for all subsequent computations. For species containing the atoms B, C, and N, the Dunning correlation consistent basis sets aug-cc-pVXZ ($X=T, Q$)^{121,122} were used. For species containing the atoms Al, Si, and P, the aug-cc-pV($X+d$)Z ($X=T, Q$)^{123,124} basis sets were used. In our preliminary computations, we found that correlating the $4s$ and $4p$ electrons only for row three atoms Ge, Ga, and As was not sufficient to accurately capture the singlet-triplet gap and the additional correlation of $3d$ electrons was needed (see Table 1). Thus, the weighted core-valence basis sets [aug-cc-pwCVXZ ($X=T, Q$)]¹²⁵ were used for Ge, Ga, and As containing species because the aug-cc-pVXZ¹²⁶ basis set parameters for Ge and Ga were obtained with the correlation of the $4s$ and $4p$ electrons only.

Table 1 Comparison of the effects of correlation on the energies and singlet-triplet (ST) gap of HGaCN⁻. A positive ST gap (ΔE_{ST}) implies a triplet ground state

Correlation	Singlet (E_h)	Triplet (E_h)	ΔE_{ST} (kcal mol ⁻¹)
$4s4p$	-2016.632961	-2016.649159	10.164
$3d4s4p$	-2017.120277	-2017.075290	-28.230
$3s3p3d4s4p$	-2017.419249	-2017.373822	-28.506
all	-2017.593425	-2017.547691	-28.698

$\Delta E_{ST} = E_{\text{singlet}} - E_{\text{triplet}}$. Correlating only the $4s$ and $4p$ electrons gives a qualitatively wrong singlet-triplet gap and reverses the energy ordering of the states. The addition of $3d$ correlation is needed to describe the correct energy ordering. At higher levels of correlation the singlet state is the ground state. Energies shown are from single point computations of HGaCN⁻ at the CCSD(T)/aug-cc-pwCVTZ level of theory with CCSD(T)/aug-cc-pVTZ optimized singlet and triplet geometries.

The Hartree-Fock density matrix elements, coupled cluster amplitudes, and lambda coefficients were converged to 10^{-9} for all molecules except singlet HGaCN⁻ at CCSD(T)/aug-cc-pwCVQZ, which was converged to 10^{-8} . The RMS gradient for the geometry optimizations was converged to 10^{-8} . A restricted Hartree-Fock (RHF) reference was used for singlet states, while a restricted open-shell Hartree-Fock (ROHF) reference was used for triplet states. The electronic structure program CFOUR 2.0¹²⁷ was used to obtain all reported geometries and harmonic vibrational frequencies except for the vibrational frequencies for triplet HGaCN, which was computed using Molpro^{128,129}. Moving forward, the set of aug-cc-pVXZ ($X=T, Q$), aug-cc-pV($X+d$)Z ($X=T, Q$) and aug-cc-pwCVXZ ($X=T, Q$) basis sets will be collectively referred to as XZ.

Energetics

Singlet-triplet (ST) energy gaps (ΔE_{ST}) defined as $E_{\text{singlet}} - E_{\text{triplet}}$, where a positive gap indicates a triplet ground state, were obtained via the focal point approach of Allen and coworkers.

This approach allows us to obtain ST gaps at the CCSDT(Q)/CBS level of theory. Single point energies at the HF, MP2, CCSD, CCSD(T), CCSDT, and CCSDT(Q) levels of theory were performed using the CCSD(T)/QZ optimized structures. The HF through CCSD(T) computations were performed using Molpro^{128,129} at the DZ, TZ, QZ, and 5Z levels. The basis set type used for each species was the same as that employed for geometry optimizations. Full CCSDT computations were performed at the TZ level using the NCC¹³⁴ module for the singlets and the VCC module for the triplets in CFOUR 2.0. CCSDT(Q) computations were performed at the DZ level using the NCC module in CFOUR 2.0 for the singlet states. CCSDT(Q) is not implemented for a ROHF reference in CFOUR 2.0, and thus for the triplet states MRCC¹³⁵ was used (CCSDT(Q)/B¹³⁶ energy was taken). Computations were performed to ensure that CFOUR 2.0 and MRCC gave identical CCSDT(Q) results for the singlet states. HF energies were extrapolated using Feller's three-point formula¹³⁷ and correlation energies with Helgaker's two-point formula.¹³⁸ For HNCN⁺, the focal point table did not satisfactorily converge at the CCSDT(Q) level of theory, and CCSDTQ computations at the DZ level were performed using the NCC module in CFOUR 2.0 for the singlets and MRCC^{135,139} for the triplets. Thus the ST energy gap reported for HNCN⁺ is at the CCSDTQ/CBS level of theory.

Additional corrections were added to the (ΔE_{ST}), including the Diagonal Born-Oppenheimer correction (ΔE_{DBOC} at the Hartree-Fock level) and harmonic zero-point vibrational energy correction (ΔE_{ZPVE}), both with CFOUR 2.0. Frozen-core corrections ($\Delta E_{\text{core}} = E_{\text{AE-CCSD(T)}} - E_{\text{CCSD(T)}}$) were computed with Dunning's aug-cc-pwCVQZ^{125,140,141} basis sets in Molpro. Scalar relativistic corrections ($\Delta_{\text{rel}} = E_{\text{AE-CCSD(T)/SF-X2C-1e}} - E_{\text{AE-CCSD(T)}}$) for the singlet and triplet states were determined by correlating all electrons using the SF-X2C-1e¹⁴² Hamiltonian as implemented in CFOUR 2.0 with the uncontracted aug-cc-pVTZ (B^- , C, N⁺, Ge⁻, As⁺), aug-cc-pV($T+d$)Z (Al⁻, Si, P⁺), and aug-cc-pwCVTZ (Ga⁻) basis sets. The uncontracted aug-cc-pVTZ basis set was used for Ge⁻ and As⁺ containing species instead of aug-cc-pwCVTZ because of convergence issues arising from linear dependency. To test the validity of this choice, we compared the relativistic corrections for singlet HGeCN using an uncontracted aug-cc-pVTZ and an uncontracted aug-cc-pwCVTZ basis set and found that there was very little difference between the two (0.8 mE_h).

The Cartesian coordinates, harmonic vibrational frequencies, and full focal point tables with absolute energies for all optimized species are included in the Electronic Supplementary Information (ESI)[†].

Assessment of Multi-Reference Character

To assess our use of single-reference methods for geometries and energetics, we performed full-valence CASSCF single point computations with 14 electrons in 13 active orbitals (14e⁻, 13o) using CCSD(T)/QZ optimized geometries for the singlet and triplet states of each HXCN species in Molpro. The aug-cc-pVTZ basis was used for X=B⁻, C, N⁺, aug-cc-pV($T+d$)Z for X=Al⁻, Si, P⁺, and aug-cc-pwCVTZ for X=Ga⁻, Ge, As⁺. Most of the singlet and triplet HXCN species showed a dominant configuration of 85% or

more. The second largest configuration was mostly small (contribution of under 2%); a few had a contribution around 3.5% and one had a contribution of 5.2% (singlet HAlCN⁻). Since none of the species displayed strong multi-reference character, our highly-correlated single-reference approach is more than sufficient to capture the electronic structure of the system. The species with the most multi-reference character from our computations is singlet HNCN⁺, with the dominant configuration having a contribution of 84% and the second dominant configuration having a contribution of 3.6%. The lack of convergence for the focal point energies of HNCN⁺ at CCSDT(Q) mentioned in the Energetics section might be due to HNCN⁺ having slightly more multi-reference character. However, the additional CCSDTQ correction recovers some of the missing correlation and is sufficient for the treatment of HNCN⁺. The two largest CASSCF coefficients and the corresponding occupation vectors for all HXCN species are included in the ESI[†].

H-X-C Angle Scan

A relaxed scan of the H-X-C angle, where X is the central divalent atom, of all HXCN species in the singlet and triplet states was performed to compare the barriers of linearity between species. Constrained geometry optimizations were performed with the H-X-C angle varying between 90° and 180° at 15° intervals. The CCSD(T) level of theory was used for the constrained geometry optimizations. To assess the multi-reference nature of the HXCN species as it changed geometries, MR-CISD+Q was also used to compute single point energies on top of CASSCF (10e⁻, 8o) constrained geometry optimizations. The aug-cc-pVTZ basis was used for X=B⁻, C, N⁺, aug-cc-pV(T+d)Z for X=Al⁻, Si, P⁺, and aug-cc-pwCVTZ for X= Ga⁻, Ge, As⁺. All computations for the scans were done using Molpro.

NBO

Natural bond orbital theory¹⁴³ was used to analyze the hybridization of relevant orbitals and give the natural bond orders. Important orbital donor-acceptor interactions were also analyzed via second order perturbation theory analysis of the NBO Fock matrix. The interaction energy between a donor orbital *i* and acceptor orbital *j* is defined as:

$$E(2) = q_i \left[\frac{F(i, j)^2}{\epsilon_j - \epsilon_i} \right]$$

where *q* is the charge, ϵ is the orbital energy, and $F(i, j)$ is the matrix element of the NBO Fock matrix. All NBO computations were performed using NBO 5.0 as interfaced in the Q-Chem¹⁴⁴ software package. B3LYP¹⁴⁵ was used for the NBO analysis with the aug-cc-pVDZ (X=B⁻, C, N⁺), aug-cc-pV(D+d)Z (X=Al⁻, Si, P⁺), and aug-cc-pwCVDZ (X= Ga⁻, Ge, As⁺) basis sets.

Results and Discussion

Geometries

Figure 3 shows the geometric parameters of the lowest lying singlet and triplet states in the nine cyano-species studied, while Figure 2 gives a pictorial representation of the comparison of the

geometry parameters across these species summarized below. A comparison of QZ geometry parameters with TZ parameters, as well as structures obtained from previous studies (when available) can be found in the ESI[†].

H-X-C Angle. For both the singlet and triplet states, the H-X-C angle generally increases as X traverses across a row. The difference is most dramatic for the first row (X=B⁻, C, N⁺), which showed a difference of 12.6° and 48.3° from X=B⁻ to X=N⁺, for the singlet and triplet states respectively. For triplet HNCN⁺ the lowest energy structure is no longer bent but linear. For the second row (X=Al⁻, Si, P⁺) in the singlet state, the angle stays almost the same (down by 0.01°) as X goes from Al⁻ to Si, then increases slightly by 1.8° for X=P⁺. In the triplet state the angle increases by 3.68° from X=Al⁻ to X=P⁺. For the third row (X=Ga⁻, Ge, As⁺) in the singlet state, the angle goes down slightly (0.13°) as X goes from Ga⁻ to Ge, then increases by 1.24° for X=As⁺. In the triplet state the angle increases by only 0.89° from X=Ga⁻ to X=As⁺. As X goes down the column the angles are generally decreasing. However, the change in the H-X-C angle from the first row to the second row (average decrease of 18.82° for the singlets and 36.43° for the triplets) is larger than the change from the second row to the third row (average decrease of 0.94° for the singlets and actually an increase of 0.70° for the triplets). Thus there is some convergence of the H-X-C angle as the size of X increases. For all nine species the H-X-C angle of the singlet state is smaller than that of the triplet state.

X-C-N Angle. The range of the X-C-N angle across the nine species is narrower than that of the H-X-C angle, varying between 171.3° and 174.6° in the singlet states and 175.1° and 180.0° in the triplet states. However, there is no discernible trend for how the X-C-N angle changes between species, other than the fact that the singlet state angles are always smaller than triplet state angles. We note that none of the angles is perfectly linear, except in the case of triplet HNCN⁺.

X-H and X-C Bonds. The X-H and X-C bonds follow the same periodic trend and will be discussed together. For both the singlet and triplet states, the X-H and X-C bonds decrease as X traverses across a row. The net decrease in all three rows were about the same. In the singlet state, the X-H and X-C bond respectively decreased by 0.188 Å and 0.312 Å as X changed from B⁻ to N⁺, 0.245 Å and 0.366 Å as X changed from Al⁻ to P⁺, and 0.153 Å and 0.295 Å as X changed from Ga⁻ to As⁺. In the triplet state, the X-H and X-C bond respectively decreased by 0.177 Å and 0.329 Å as X changed from B⁻ to N⁺, 0.189 Å and 0.301 Å as X changed from Al⁻ to P⁺, and 0.066 Å and 0.175 Å as X changed from Ga⁻ to As⁺. The bond length increases as X goes down a column but at a decreasing rate, similar to the H-X-C angle. The only exception is the slight decrease in the X-C bond length from 1.992 Å to 1.987 Å going from X=Al⁻ to Ga⁻. Predictably, the X-H bond is always shorter compared to the X-C bond in a given species.

C-N Bond. The C-N bonds show the smallest variation between species, lying between 1.17 Å and 1.18 Å in the singlet states and 1.17 Å and 1.19 Å in the triplet states for all species except HNCN⁺, which has longer C-N bonds (1.223 Å for the

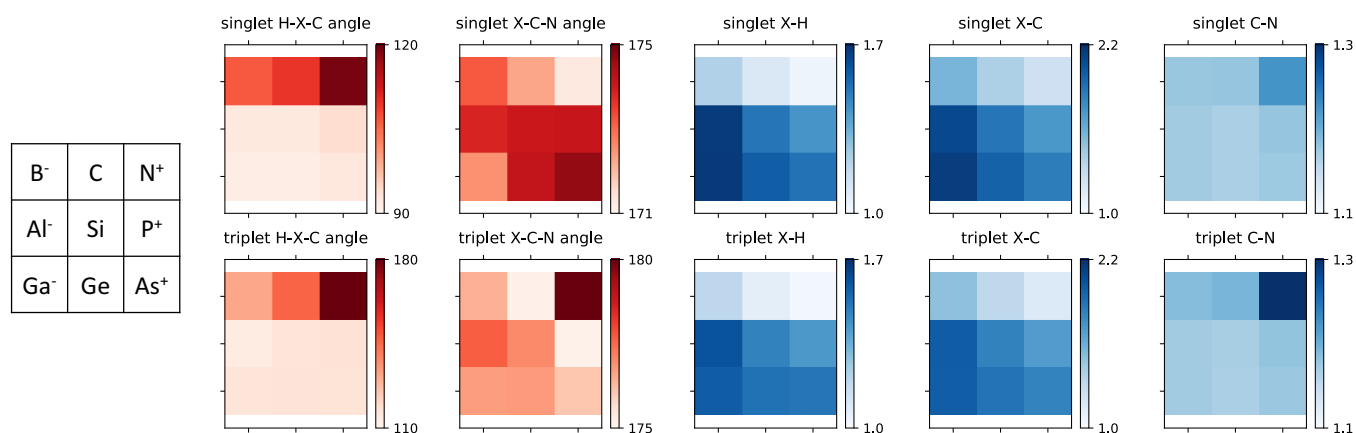


Fig. 2 Pictorial comparison of HXCN geometric parameters. The three by three grid shown for each geometrical parameter represents the nine species HXCN studied, with X shown on the leftmost grid. The color bar beside each grid shows the range of values depicted. Angles are shown in degrees (°) and bond distances are shown in angstroms (Å). Increasing color intensity represents an increase in the value of the geometric parameter.

singlet and 1.306 Å for the triplet). The exception is because HNCN^+ does not have a carbene-like electronic structure, which will be discussed in detail in later sections. It is interesting to note that the shortest C–N bonds are seen in HSiCN and HGeCN , both with bonds of around 1.167 Å for the singlet and triplet states. The C–N bond is shorter than the H–X bond in all cases except for singlet and triplet HCCN and HNCN^+ , and shorter than the X–C bond in all species except triplet HNCN^+ . The C–N bond length in triplet HNCN^+ especially suggests that the bonding is less sp in nature like the other species and has more sp^2 character brought about by its linear geometry. This observation will be discussed more thoroughly in later sections.

Singlet-Triplet Gaps

Table 2 shows the focal pointed singlet-triplet (ST) gap ($\Delta E_{ST} = E_{\text{singlet}} - E_{\text{triplet}}$) for all nine HXCN species. The ST gap shows convergence at the CCSDT(Q) level of theory for all species except HNCN^+ , which required an additional CCSDTQ computation to reach satisfactory convergence (see Methods section). The magnitude of ZPVE corrections to the ST gap are below 0.4 kcal mol⁻¹ for all of the species except HGaN^- , which has a ZPVE correction of -0.68 kcal mol⁻¹. The magnitude of frozen core corrections fall below 0.5 kcal mol⁻¹ for all species. The relativistic corrections to the ST gap varied the most. In the first row (X=B⁻, C, N⁺), the relativistic corrections were the smallest (less than 0.1 kcal mol⁻¹ in magnitude). In the second row (X=Al⁻, Si, P⁺), the relativistic corrections increased significantly, and varied between -0.22 kcal mol⁻¹ for HAlCN^- and -0.44 kcal mol⁻¹ for HPCN^+ . In the third row (X=Ga⁻, Ge, As⁺), the relativistic corrections were the largest, and varied between -1.69 kcal mol⁻¹ for HGaN^- and -2.09 kcal mol⁻¹ for HGeCN . The singlet state was more affected by the relativistic correction compared to the triplet state in all cases. This increase in relativistic correction is expected as relativistic effects become more important with heavier atoms.¹⁴⁷ The DBOC corrections are the smallest in magnitude, with most having a correction below 0.1 kcal mol⁻¹

and HNCN^+ having a DBOC correction of 0.2 kcal mol⁻¹.

As X moves from B⁻ to C to N⁻ in the first row, the ST gap increases from 3.49 kcal mol⁻¹ for HBCN^- to 11.86 kcal mol⁻¹ for HCCN to 22.64 kcal mol⁻¹ HNCN^+ , showing an increasing preference for the triplet state. Our computed CCSDT(Q)/CBS ST gap for HBCN^- is slightly lower than the value obtained by Liebman and coworkers [3.94 kcal mol⁻¹ with CCSD(T)/DZP(d)//MBPT(2)/DZP(d)].⁵¹ For HCCN , the computed CCSDT(Q)/CBS ST gap is lower than the 13.8 kcal mol⁻¹ gap computed at the QCISD(T)/D95** level of theory⁷⁸, but higher than the gaps obtained by two other studies [9.93⁸⁶ at QCISD(T)/6-311++G** and 7.61⁸⁸ with the G2 composite theory]. For HNCN^+ , the computed CCSDT(Q)/CBS ST gap is lower than a multi-reference result by Antoniotti and coworkers by 2 kcal mol⁻¹ [24.6 kcal mol⁻¹ at MR-CISD(Q)/6-311G**//CASSCF(8e⁻,8o)/6-31G*].¹¹⁶

Moving from the first row to the second row, there is a switch in the ordering of the states. Unlike all the species in the first row, in the second and third rows the singlet state is now the favored state, and the sign of the ST gap is now negative instead of positive. As X moves from Al⁻ to Si to P⁺, the ST gap increases in magnitude from -20.34 kcal mol⁻¹ for HAlCN^- to -26.63 kcal mol⁻¹ for HSiCN to -26.73 kcal mol⁻¹ for HPCN^+ . Like the first row, the magnitude of the gap in the second row gets larger moving from left to right, but this time the singlet state is increasingly favored instead of the triplet. The change in the ST gaps between species are not as dramatic in the second row. The magnitude of change in the ST gap from HBCN^- to HCCN is 8.37 kcal mol⁻¹, and from HCCN to HNCN^+ is 10.78 kcal mol⁻¹. In contrast, the magnitude of change in the ST gap from HAlCN^- to HSiCN is 6.29 kcal mol⁻¹, and from HSiCN to HPCN^+ is only 0.10 kcal mol⁻¹. Compared to previous results, our computed CCSDT(Q)/CBS ST gap for HSiCN (-26.63 kcal mol⁻¹) is close to that of Flores and coworkers⁹⁷ [-26.51 kcal mol⁻¹ at CCSD(T)/CBS//B3LYP/6-311G**] and Kalcher⁹⁹ (-26.22 kcal mol⁻¹ at ACPF/aug-cc-pVTZ). It is larger than both previous DFT [-24.55 kcal mol⁻¹ at B3LYP/6-31G(d)]⁹⁸ and

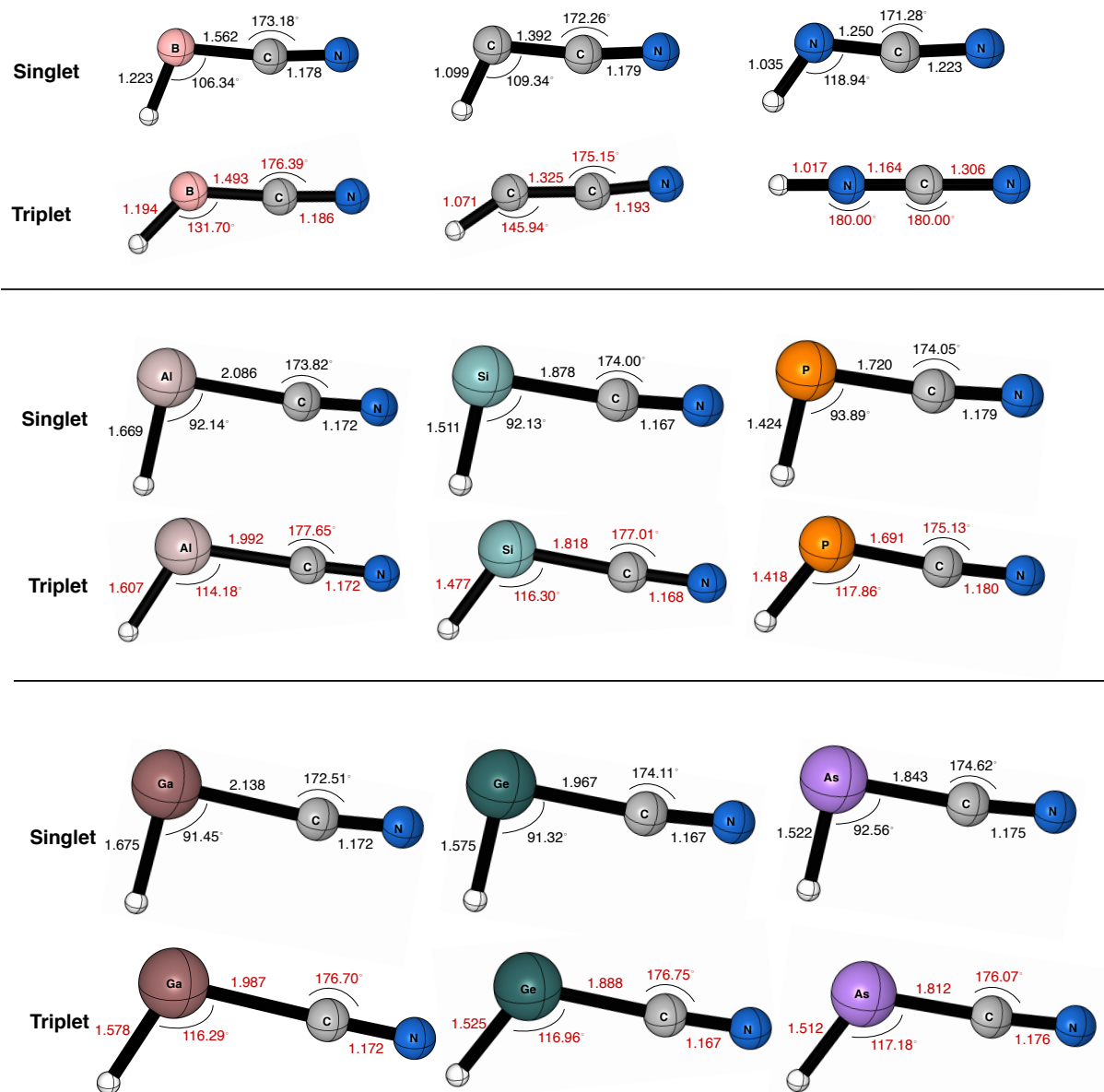


Fig. 3 Geometries at the CCSD(T) level of theory with the aug-cc-pVTZ basis sets for the first row, aug-cc-pV(Q+d)Z for the second row, and aug-cc-pwCVQZ for the third row. In a given row, the top geometry shows values (black) for the lowest lying $^1A'$ state while the bottom show values (red) for the lowest lying $^3A''$ state. The H-X-C-N dihedral angle is 180° in all cases, i.e., each structure is planar. Graphics were made with CYLview.¹⁴⁶

multi-reference $[-22.83 \text{ kcal mol}^{-1}$ at CASPT2 ($14e^-$, $13o$)/aug-cc-pVTZ]⁹⁶ results. The CCSDT(Q)/CBS ST gap for HPCN⁺ ($-26.73 \text{ kcal mol}^{-1}$) is much smaller than magnitude than a previously obtained result of $-30.44 \text{ kcal mol}^{-1}$ using the G3 composite method.¹¹⁷

The ST gaps of the third row show a further increase in preference for the singlet state compared to the second row, evidenced by the more negative ST gaps in the HXCN ($X = \text{Ga}^-, \text{Ge}, \text{As}^+$)

species. Like the second row, there is a decreasing rate of change in the ST gaps moving from left to right. The ST gap changed by $6.29 \text{ kcal mol}^{-1}$ between HGaCN⁻ and HGeCN, decreasing from $-26.78 \text{ kcal mol}^{-1}$ to $-33.46 \text{ kcal mol}^{-1}$. Going from HGeCN to HAsCN⁺, the change is now only $0.38 \text{ kcal mol}^{-1}$, increasing from $-33.46 \text{ kcal mol}^{-1}$ to $-33.08 \text{ kcal mol}^{-1}$. The change from HGeCN to HAsCN⁺ is a break from the trend of increasing ST gap magnitudes seen in the first and second rows. It is interesting

Table 2 Incremental focal point singlet-triplet (ST) gaps for the HXCN species. Energies are in kcal mol⁻¹. A positive ST gap implies a triplet ground state ($\Delta E_{ST} = E_{\text{singlet}} - E_{\text{triplet}}$). Single point energies were performed on the singlet and triplet HXCN geometries optimized at the CCSD(T)/QZ level of theory. Each column shows the incremental change (δ) in ST energy gap from the previous column. Numbers shown in brackets were not directly computed. The final ΔE_{ST} is given with corrections as follows: $\Delta E_{ST} = \Delta E_{ST}[\text{CCSDT(Q)/CBS}] + \Delta E_{ZPVE} + \Delta E_{\text{core}} + \Delta E_{\text{rel}} + \Delta E_{\text{DROC}}$. Additional details on these corrections are given in the Methods section. The ST gap was extrapolated to the CCSDTQ/CBS level of theory for HCN⁺

	HBCN ⁻			HCCN			HNCN ⁺		
	HF	+ δ MP2	+ δ CCSD + δ CCSD(T) + δ CCSDT + δ CCSDT(Q)	HF	+ δ MP2	+ δ CCSD + δ CCSD(T) + δ CCSDT + δ CCSDT(Q)	HF	+ δ MP2	+ δ CCSD + δ CCSD(T) + δ CCSDT + δ CCSDT(Q)
aug-cc-pVDZ	+13.33	-5.84	-2.76 -0.95	+13.96	+1.31	-2.25 -1.13	+43.03	-13.70	-0.61 -4.54
aug-cc-pVTZ	+13.48	-6.56	-2.14 -0.93	+14.55	+0.38	-1.97 -1.10	+43.94	-14.97	-0.29 -4.78
aug-cc-pQZ	+13.51	-6.93	-1.84 -0.93	+14.59	-0.03	-1.78 -1.08	+43.97	-15.46	-0.07 -4.82
aug-cc-pwSZ	+13.52	-7.11	-1.70 -0.94	+14.60	-0.26	-1.66 -1.08	+43.99	-15.75	+0.06 -4.84
CBS Limit	[+13.52]	[-7.30]	[-1.55] [-0.94]	[+14.61]	[-0.50]	[-1.54] [-1.08]	[+44.00]	[-16.06]	[+0.21] [-4.86]
			$\Delta E_{ST} = 3.44 - 0.33 + 0.37 - 0.04 + 0.06 = 3.49$			$\Delta E_{ST} = 11.12 + 0.25 + 0.47 - 0.07 + 0.09 = 11.86$			$\Delta E_{ST} = 22.30 - 0.20 + 0.42 - 0.08 + 0.20 = 22.64$
aug-cc-pVDZ	-5.56	-9.49	-3.57 -0.41	-11.56	-9.43	-3.47 -0.43	-15.28	-6.21	-3.06 -0.65
aug-cc-pVTZ	-5.28	-10.87	-2.70 -0.43	-11.39	-10.99	-2.70 -0.45	-15.07	-7.96	-2.51 -0.61
aug-cc-pQZ	-5.13	-11.34	-2.26 -0.43	-11.18	-11.61	-2.25 -0.46	-14.95	-8.61	-2.16 -0.59
aug-cc-pwSZ	-5.12	-11.63	-2.02 -0.43	-11.19	-11.91	-2.02 -0.46	-14.98	-8.90	-1.96 -0.58
CBS Limit	[-5.12]	[-11.92]	[-1.78] [-0.44]	[-11.21]	[-12.22]	[-1.78] [-0.45]	[-15.01]	[-9.21]	[-1.74] [-0.57]
			$\Delta E_{ST} = -19.26 - 0.36 - 0.52 - 0.22 + 0.02 = -20.34$			$\Delta E_{ST} = -25.64 - 0.19 - 0.45 - 0.39 + 0.03 = -26.63$			$\Delta E_{ST} = -26.44 + 0.34 - 0.24 - 0.44 + 0.06 = -26.73$
aug-cc-pVDZ	-12.13	-9.60	-1.55 -0.63	-18.78	-9.71	-1.18 -0.61	-21.24	-7.58	-0.71 -0.70
aug-cc-pVTZ	-11.96	-10.93	-0.53 -0.78	-18.49	-11.33	-0.20 -0.75	-20.94	-9.37	+0.07 -0.76
aug-cc-pQZ	-11.87	-11.40	-0.11 -0.83	-18.45	-11.83	+0.20 -0.79	-20.91	-9.85	+0.39 -0.78
aug-cc-pwSZ	-11.85	-11.61	+0.07 -0.84	-18.44	-12.06	+0.38 -0.80	-20.91	-10.09	+0.55 -0.79
CBS Limit	[-11.85]	[-11.61]	[+0.26] [+0.11]	[-18.44]	[-12.30]	[+0.56] [-0.81]	[-20.91]	[-10.33]	[+0.71] [-0.79]
			$\Delta E_{ST} = -24.29 - 0.68 - 0.15 - 1.69 + 0.02 = -26.78$			$\Delta E_{ST} = -30.95 - 0.17 - 0.29 - 2.09 + 0.04 = -33.46$			$\Delta E_{ST} = -31.20 + 0.34 - 0.28 - 1.99 + 0.05 = -33.08$

to note that the CCSDT(Q)/CBS ST gaps without additional corrections do show an increase in ST gap magnitude from HGeCN to HAsCN⁺ (−30.95 kcal mol^{−1} to −31.20 kcal mol^{−1}). The two main sources for an overall lower ST gap in HGeCN thus come from: 1. a negative contribution from the ZPVE correction in HGeCN (−0.17 kcal mol^{−1}) combined with a positive ZPVE correction in HAsCN⁺ (0.34 kcal mol^{−1}); and 2. a relativistic correction in HGeCN that is more negative (−2.09 kcal mol^{−1}) than the relativistic correction in HAsCN⁺ (−1.99 kcal mol^{−1}). Our computed CCSDT(Q)/CBS ST gap for HGeCN (−33.46 kcal mol^{−1}) is slightly lower than the −32.83 kcal mol^{−1} gap reported by Kassae and coworkers using the G2 composite method.¹⁰⁹ A discussion of these general trends will be made in the following section.

Origins of the ST Gap

As mentioned in the introduction, the magnitude of the ST gap in carbenes can largely be explained by understanding the nature of the two relevant orbitals for the two nonbonding electrons on the divalent atom. In our case, the HXC�N species has C_s geometry, and subsequently the two relevant orbitals are an in-plane *a'* orbital that has mixed *s*- and *p*-character, and an out-of-plane *a''* orbital that has largely *p*-character. The relation between these orbitals and the ST gap can be summarized as follows: the more *s*-character the *a'* orbital has (leading to a more bent H–X–C angle), the larger the energy separation between the *a'* and *a''* orbitals, and the more the singlet state is favored.

Schleyer and coworkers in their comparative study on silylenes vs. carbenes used these principles to explain the differences between the two species.^{17,18} First, they pointed out that the nonbonding electrons in silicon are often in orbitals that have more *s*-character compared to carbon. Second, they compare the energy gap between the singly occupied molecular orbitals (SOMO) in the triplet state for CH₂ and SiH₂, citing the larger gap in SiH₂ as the reason for its preference for a singlet ground state.

In Figure 4, we quantify these two characteristics, namely, the percentage of *s*-character in the *a'* orbital in the singlet state and the energy gap between the two SOMOs in the triplet state and plot them against the ST gap for the nine species we are presently studying. We see that the observations made for carbenes and silylenes carry through to the other carbene derivatives. There is a strong correlation between the ST gap with both the percentage of *s*-character in the *a'* orbital (R²=0.975) and SOMO energy gap (R²=0.945) in the triplet state. As expected, the species that strongly favor a singlet ground state have both a higher percentage of *s*-character in their *a'* orbital, and a larger SOMO energy gap.

Barrier to Linearity

As mentioned in the introduction, the barrier to linearity for triplet HCCN is well studied both computationally and experimentally as evidence of its bent but quasilinear character. In Figure 5 we compare the barrier to linearity across the singlet and triplet states of each HXC�N species, showing how the relative energies vary as the H–X–C angle increases from 90° to 180°. Both single-reference and multi-reference methods are used, although

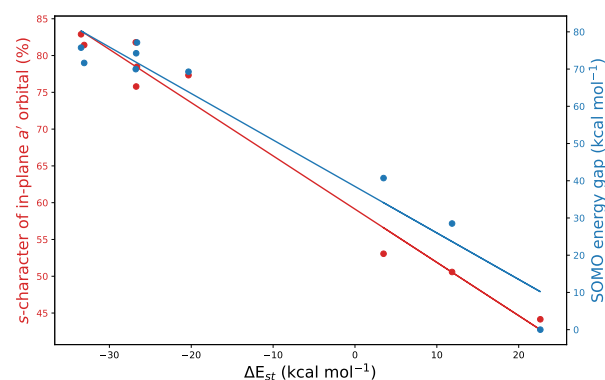


Fig. 4 The correlation between HXC�N ST gap and both the percentage of *s*-character in the in-plane *a'* lone pair orbital in the singlet state and the SOMO energy gap computed for the triplet state. *s*-character is obtained through NBO computations as described in the Methods section. Orbital energies for the SOMO energy gap were computed at the RHF/QZ level of theory. R²=0.975 for the percentage of *s*-character in the in-plane *a'* lone pair orbital vs. ST gap, R²=0.945 for SOMO energy gap vs. ST gap

for the most part, the relative energies between the singlet and triplet states of a given species does not change much between the two methods. The only significant difference is in the singlet state of HCCN and HNCN⁺, in which MR-CISD+Q shows a lower energy gap relative to the triplet compared to CCSD(T) as the H–X–C angle approaches linearity. We can make several observations:

- Compared to triplet HCCN, the rest of the HXC�N species studied are less floppy near their ground state geometries, with triplet HNCN⁺ being decidedly linear and the others decidedly bent.
- Moving down the column, the barrier to linearity increases dramatically for the singlet and somewhat less so for the triplet. A smaller H–X–C angle at the optimized geometry leads to a much larger barrier to linearity.
- The angle at which the state ordering is switched increases down the column. In the first row, the switch in state ordering happens at around 105° for HBCN[−] and HCCN and less than 90° for HNCN⁺. Meanwhile, the switch happens at around 140° for the species in the second row and 150° for the species in the third row.
- When the H–X–C angle is at 180°, the triplet state is always lower than the singlet state. When H–X–C angle is at 90°, the singlet is always lower than the triplet state (except for HNCN⁺). This is expected given that as a linear geometry is reached the energy gap between the *a'* and *a''* orbitals on the divalent atoms decreases, and the triplet state is increasingly favored.
- While the ST gap in the optimized geometries varies wildly as discussed in previous sections, the gap between the states

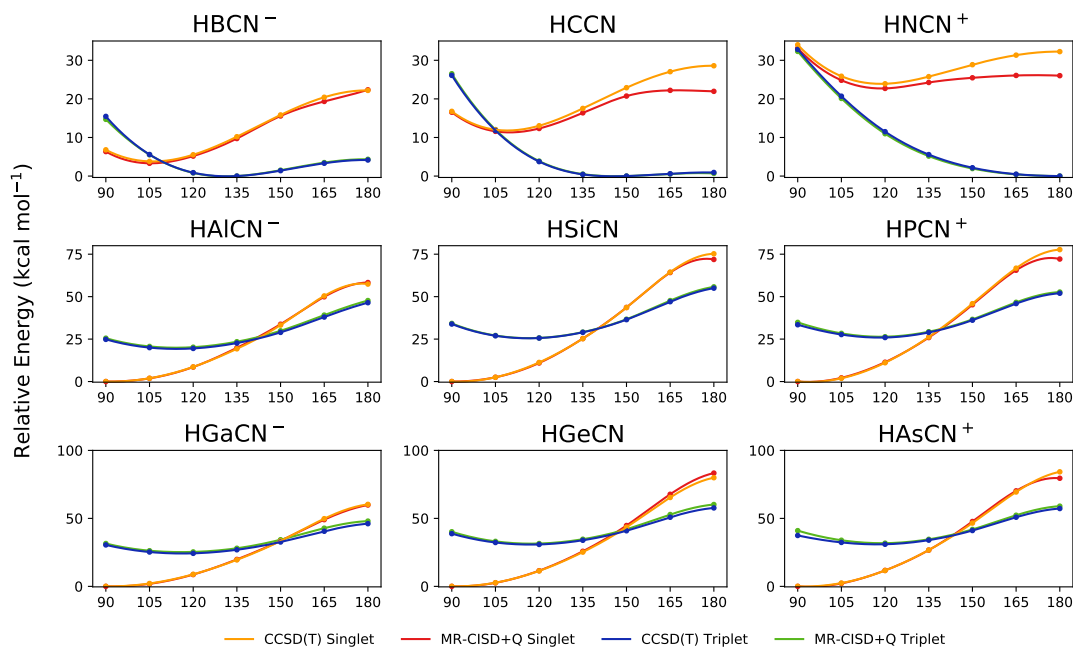


Fig. 5 Relaxed scan of the H-X-C angles, where X is the central divalent atom. The energies were obtained by constrained optimizations at the CCSD(T) level of theory. MR-CISD+Q single point energies were computed following CASSCF (10o, 8e⁻) constrained geometry optimizations. The basis sets used are described in the Methods section. Relative energies (kcal mol⁻¹) of the singlet and triplet states at both CCSD(T) and MR-CISD+Q levels of theory are shown against the H-X-C angle in degrees. The reference energy for each level of theory is the lowest energy point out of both the singlet and triplet states for each species.

at a linear geometry falls within a narrower range between the species. Moreover, as the previous point mentions, the ST gaps are all positive because the triplet state is always lower than the singlet state when the H-X-C angle is at 180°. The first row species HBCN⁻ (18.04 kcal mol⁻¹), HCCN (27.65 kcal mol⁻¹), and HNCN⁺ (32.25 kcal mol⁻¹) display the largest gaps, while the second row species HAlCN⁻ (10.96 kcal mol⁻¹), HSiCN (20.24 kcal mol⁻¹), HPCN⁺ (25.70 kcal mol⁻¹) display the smallest gaps. The third row species HGaCN⁻ (14.18 kcal mol⁻¹), HGeCN (22.22 kcal mol⁻¹), and HAsCN⁺ (27.00 kcal mol⁻¹) fall in between the two. Across a row, the energy gap at the linear geometry increases on average from anions to neutral species to cations.

Comparing the ST gap of HXCN and XH₂

We also wanted to see how the substitution of a cyano (CN) group influences the ST gap of the HXCN compared to its parent derivative XH₂. Table 3 compares the focal-pointed ST gap of HXCN and XH₂ at the CCSD(T)/CBS level of theory using the optimized CCSD(T) geometries with either a TZ or QZ basis set. The difference between using a TZ or QZ geometry makes a difference of at most 0.09 kcal mol⁻¹ in the ST gap for the HXCN species and 0.07 kcal mol⁻¹ for the XH₂ species. Moving forward we will focus on the CCSD(T)/CBS gap at the QZ geometry.

The trends for the ST gap of the XH₂ species shown in Table 3 are similar to those obtained by Cramer and coworkers.

Table 3 Singlet-Triplet Energy Differences for XH₂ and HXCN

Species	XH ₂		HXCN	
	TZ	QZ	TZ	QZ
B ⁻	-0.30	-0.23	3.47	3.49
C	8.95	8.99	11.81	11.86
N ⁺	29.14	29.18	22.66	22.64
Al ⁻	-14.64	-14.64	-20.43	-20.34
Si	-21.52	-21.51	-26.64	-26.63
P ⁺	-18.68	-18.65	-26.74	-26.73
Ga ⁻	-18.59	-18.59	-26.76	-26.78
Ge	-26.18	-26.20	-33.49	-33.46
As ⁺	-24.33	-24.28	-33.11	-33.08

Singlet-Triplet (ST) gaps defined as $\Delta E_{ST} = E_{\text{singlet}} - E_{\text{triplet}}$ and shown in kcal mol⁻¹. The ST gaps shown were extrapolated to CCSDT(Q)/CBS on a CCSD(T)/TZ (TZ columns) or CCSD(T)/QZ (QZ columns) geometry. The ST gaps for the X=N⁺ species were extrapolated to the full CCSDTQ/CBS level of theory.

ers.²⁹ For BH₂⁻, they predict a triplet ground state ($\Delta E_{ST} = 0.1$ kcal mol⁻¹), while we predict a singlet ground state ($\Delta E_{ST} = -0.23$ kcal mol⁻¹). For X=Si and onwards, our ST gaps are consistently 2–4 kcal mol⁻¹ larger in magnitude compared to their MR-CISD+Q values. Cramer and coworkers give an excellent discussion regarding the periodic trends seen in the ST gaps of XH₂, which will be summarized here. In the first row, we start with BH₂⁻, whose lowest singlet and triplet states are nearly degenerate. As we move across the row, the increase in nuclear charge leads to a contraction of all the orbitals and subsequently

increased Coulombic repulsion. The triplet state is thus increasingly favored, because the promotion of an electron from the lone pair orbital on the divalent atom relieves this Coulombic repulsion. For later rows, this effect is not as important because the valence orbitals of higher quantum levels are more diffuse, and the need to relieve Coulombic repulsion is not as large. Instead, the dominant effect becomes the Coulombic attraction between electrons and the nucleus. Electrons in the in-plane lone pair orbital are closer to the nucleus than the out-of-plane lone pair orbital, and thus the singlet state is increasingly favored as nuclear charge (and the strength of Coulombic attraction) increases going across the row. The general trend for the ST gap in XH_2 holds when we replace H with CN, and the same periodic arguments apply. We will turn our attention now to the differences between XH_2 and HXCN.

The differences between the ST gap of HXCN and XH_2 are the most varied in the first row. The $X=B^-$ species is the only one that switches the state ordering between BH_2^- and $HBCN^-$, moving from a singlet ground state (albeit only $0.23 \text{ kcal mol}^{-1}$ lower) to a triplet ground state. In the $X=C$ species the ST gap also increases going from CH_2 to HCCN, showing that a triplet ground state is more favorable with the substitution of the cyano group. In the $X=N^+$ species, the ST gap actually decreases going from NH_2^+ to $HNCN^+$. Although the triplet is still the ground state in $HNCN^+$, its energy separation from the singlet state is $6.5 \text{ kcal mol}^{-1}$ less than in NH_2^+ . For $X=Al^-$, Si, P^+ and $X=Ga^-$, Ge, As^+ , the singlet ground state is maintained between XH_2 and HXCN, and the energy separation between the singlet and triplet states is consistently enlarged. The electronic ground state is further stabilized with the substitution of the CN group.

Isodesmic Analysis

In order to gain insight into the origin of the differences between the ST gaps of HXCN and XH_2 , we can isolate how the substitution of CN separately affects the singlet and triplet states. To this end, we can study an isodesmic bond separation reaction originally introduced by Pople and coworkers¹⁴⁸ and used for carbenes by Schleyer and coworkers¹⁸ and more recently by Eckhardt and Schreiner¹⁴⁹. In an isodesmic reaction, the number of a given type of bond stays the same between products and reactants, but their connectivity changes. Equations 1 and 2 respectively give the bond separation reaction for the singlet and triplet states of the cyano-species:



The bond separation energy for these reactions measures the effect of replacing a hydrogen with CN in XH_2 . A negative bond separation energy indicates that the substitution of the cyano group in XH_2 provides a stabilizing interaction, while a positive bond separation energy indicates that the cyano group provides a destabilizing interaction.

Table 4 gives the bond separation energies for the singlet and triplet states. We note that for each species, the difference between the singlet and triplet bond separation energies mirrors

the difference between the ST gaps of XH_2 and HXCN (Table 3). Thus the isodesmic analysis is a way to decompose the difference between the ST gaps of HXCN and XH_2 into separate contributions from the singlet and triplet states. There are three types of patterns of decomposition seen across the nine species. First, the bond separation energy is positive for the singlet state and negative for the triplet state. This pattern only applies for the case of $X=B^-$. Since the singlet and triplet states in BH_2^- are nearly degenerate, the stabilizing interaction provided by the cyano group for the triplet state results in a net preference for the triplet state in $HBCN^-$. Second, the bond separation energy is negative for the singlet state and positive for the triplet state. This case applies to both $X=Al^-$, Ga^- where the magnitude of the singlet state bond separation energy is less than the magnitude of the triplet state bond separation energy, and $X=Si$, Ge where the magnitude of the singlet state bond separation energy is more than the magnitude of the triplet state bond separation energy. Third, both states have a negative bond separation energy. In $X=C$, the bond separation energy is greater in magnitude in the triplet state than the singlet state while in $X=N^+$, P^+ , and As^+ , the opposite is true. This explains the decrease in preference for the triplet state in $HNCN^+$ as compared to NH_2^+ .

Table 4 Isodesmic Bond Separation Energies

	B^-	C	N^+
singlet	0.89	-11.46	-64.53
triplet	-2.88	-14.32	-58.04
	Al^-	Si	P^+
singlet	-0.77	-3.76	-12.94
triplet	5.02	1.36	-4.88
	Ga^-	Ge	As^+
singlet	-2.82	-5.33	-11.52
triplet	5.35	1.97	-2.74

Bond separation energies are given in kcal mol^{-1} and are obtained with Equation 1 and 2 in the main text for the singlet and triplet states, respectively. Each species was optimized at the CCSD(T)/TZ level of theory. Focal point extrapolation and additional corrections were performed for all molecules in the same manner as HXCN, described in the Methods section to give CCSDT(Q)/CBS energies for every species except $X=N^+$ (CCSDTQ/CBS energies). Table 3 shows that using CCSD(T)/TZ optimized geometries gives similar ST gaps as compared extrapolations completed using a CCSD(T)/QZ geometry.

NBO Analysis

NBO analysis can be used to help explain how interactions between X and CN give rise to the isodesmic bond separation energies seen in the previous section (Figure 6). In the singlet state, the natural bond order of X-C increases going across a row and decreases down a column while the bond order of C-N shows the opposite trend. The change in bond order transitioning from the neutral species to cations in every row is much more dramatic than going from anions to the neutral species. Weinhold's second order NBO analysis¹⁴³ points to two orbital interactions responsible for this trend (The values from the second order NBO analysis are shown in the ESI[†]):

has large contributions for the other cations in the series (12% for HPCN⁺ and 10% for HAsCN⁺). HCCN displays significant weight for the X=C=N resonance structure (11%), but the other neutral HXCN species do not (2.6% for HSiCN and 2.3% for HGeCN). The X=C=N resonance has little weight in the overall structure for all of the anions (2.4%, 0.5%, and 0.5% respectively for HBCN⁻, HAlCN⁻, and HGaCN⁻).

We conclude that in the singlet state, the cyano group provides stabilizing interactions by the pulling of electron density away from the *a'* in-plane LP orbital and consequently giving rise to additional resonance structures (X=C=N). The bond separation energies for the singlet states from the isodesmic analysis are well correlated with the X-C bond order and the weight of the resonance structures, not only in the trend but also the magnitude. The most dramatic example of this is seen going from HCCN to HNCN⁺. The singlet isodesmic bond separation energy goes from -11.5 kcal mol⁻¹ in HCCN to -64.5 kcal mol⁻¹ in HNCN⁺ as the X-C bond order goes from 1.21 to 1.91 and the weight of the X=C=N resonance structure increases from 11% to 20%.

Several major differences can be seen when comparing the bond orders of the singlet and triplet states. First, we notice a significant decrease on lone pair (LP) occupancy of X in the triplet states, compared to the singlet states for the first row. While the LP occupancy of the other rows decrease going from the singlet to triplet state, the difference is much smaller. Second, the X-C bond order is consistently larger in the triplet, while the C-N bond order is consistently smaller. However, the overall trend between species is the same.

In the triplet state, the in-plane *a'* and out-of-plane *a''* orbitals are partially filled and have roles as both donor and acceptor. There are four important donor-acceptor orbital interactions in the triplet state:

1. The donation of electron density from the out-of-plane (oop) *a''* orbital to the out-of-plane anti-bonding C-N orbital (*a''* → oop-CN*);
2. The donation of electron density from the in-plane (ip) *a'* orbital into the in-plane anti-bonding C-N orbitals (*a'* → ip-CN*);
3. The donation of electron density from the out-of-plane bonding C-N orbital into the out-of-plane *a''* orbital (oop-CN → *a''*);
4. The donation from the in-plane bonding C-N orbitals into the in-plane *a'* orbital (ip-CN → *a'*).

In the first row, donation of electron density from the *a'* and *a''* orbitals to the C-N anti-bonding orbitals result in the relatively large bond orders as well as the negative isodesmic bond separation energy for HBCN⁻. The additional back donation of electron density from the C-N bonding orbitals to the *a'* and *a''* orbitals in HCCN is what gives it a larger bonding order and a more negative isodesmic bond separation energy compared to HBCN⁻. For HNCN⁺, an interesting phenomenon is observed. The divalent nitrogen (N1) forms a triple bond with the carbon, leaving the terminal nitrogen (N4) with the unpaired electrons. The bond order of triplet HNCN⁺ reflects this: the N1-C bond order (2.45) is larger than the C-N4 bond order (1.54). The linear geometry allows for maximum orbital interactions and results in large donor-acceptor orbital interaction energies.

For the other two rows, the *a''* → oop-CN* interaction energy

is bigger than the *a'* → ip-CN* interaction energy, and increases across a row. The oop-CN → *a''* and ip-CN → *a'* interaction energies also increase across a row and are only significant in the cations HPCN⁺ and HAsCN⁺. The increase of these interactions across a row causes a subsequent increase in bond order. The isodesmic bond separation energies follow suit: triplet AlH₂⁻ and GaH₂⁻ is favored over triplet HAlCN⁻ and HGaCN⁻ by 5 kcal mol⁻¹, but triplet SiH₂ and GeH₂ is only favored over triplet HSiCN and HGeCN by 2 kcal mol⁻¹. The additional orbital interactions in the cations cause the bond separation energy to switch signs to favor triplet HPCN⁺ and HAsCN⁺ over PH₂⁺ and AsH₂⁺ by 4.9 kcal mol⁻¹ and 2.7 kcal mol⁻¹ respectively.

In both the singlet and the triplet states, the NBO results for the anion and neutral species are more similar than the neutral and cation species. The overall increase of the strength of orbital interactions in the cation species could be due to the combination of the increase in nuclear charge and the removal of an electron for a formal positive charge. The interesting role of the terminal nitrogen atom in singlet and triplet HNCN⁺ and the overall direction of electron density toward the X-C bond is probably related to the fact that nitrogen has a higher electronegativity than carbon.

Conclusions

We have presently performed the most comprehensive and reliable study to date on the lowest lying singlet and triplet states of the HXCN species. Our results not only elucidate the periodic trends of the HXCN species but can provide insight into the behavior of other carbene species upon substitution of the divalent carbon. We summarize several key observations here:

1. HBCN⁻, HCCN, and HNCN⁺ have triplet ground states while the other molecules have singlet ground states. The first row shows the most dramatic change in ST gaps and geometrical parameters.
2. Orbital arguments used previously in the literature to explain the ground state preference of carbenes have been quantified. The singlet-triplet gaps of the nine HXCN species studied showed strong correlations both to the SOMO energy gaps in the triplet states and the percentages of *s*-character in the in-plane *a'* orbital in the singlet state.
3. Compared to HCCN, there are larger barriers to linearity for the other HXCN species.
4. The singlet-triplet gaps of HXCN are almost always larger in magnitude than their parent XH₂ molecules. The HNCN⁺ ST gap is smaller than the NH⁺ ST gap. The ground state remains the same between HXCN and XH₂ for all pairs except X=B⁻, switching from a singlet to a triplet from BH₂⁻ to HBCN⁻.
5. Isodesmic and NBO analysis show that the differences in ST gaps between HXCN and XH₂ originate from the strength of the interaction between the in-plane *a'* orbital/out-of-plane *a''* orbital on X and the bonding/anti-bonding C-N orbital.
6. HNCN⁺ represents an outlier among the nine species. It has the most positive ST gap, and the most unusual singlet (biggest H-X-C angle) and triplet (completely linear) geometries. NBO analysis shows that electron density is pulled away from the C-N bond by the divalent nitrogen cation (N1). The situation in the

triplet state is so extreme that the N1–C bond order is bigger than the C–N bond order, and the orbitals of nonbonding electrons are located at the terminal nitrogen atom instead of N1. Its peculiar behavior might stem from the fact that nitrogen is the most electronegative among the nine choices of X, and the only one that is more electronegative than carbon.

Given the relevance of HCCN and HNCN⁺ in atmospheric chemistry and the longstanding experimental interest in carbene substitutes, we hope our study will inform future experimental and computational work.

Conflicts of interest

There are no conflicts to declare.

Acknowledgements

B.Z.A. thanks Adam Abbott for helpful discussions and Dr. Justin Turney for his careful reading of the manuscript. This research was supported by the U.S. Department of Energy, Office of Basic Energy Sciences, Fundamental Interactions Branch, Computational and Theoretical Chemistry (CTC) program, Grant DE-SC0018412.

Notes and references

- C. F. Bender and H. F. Schaefer, *J. Am. Chem. Soc.*, 1970, **92**, 4984–4985.
- C. F. Bender, H. F. Schaefer, D. R. Franceschetti and L. C. Allen, *J. Am. Chem. Soc.*, 1972, **94**, 6888–6893.
- C. Wentrup, *Angew. Chem. Int. Ed.*, 2018, **57**, 11508–11521.
- B. A. Shainyan, A. V. Kuzmin and M. Y. Moskalik, *Comput. Theor. Chem.*, 2013, **1006**, 52–61.
- P. S. Skell and A. Y. Garner, *J. Am. Chem. Soc.*, 1956, **78**, 5430–5433.
- J. S. Hine, *Divalent Carbon*, Ronald Press Co., New York, 1964.
- W. Kirmse, *Carbene Chemistry*, Academic Press, New York, 2nd edn, 1971, vol. 1.
- D. Bourissou, O. Guerret, F. P. Gabbaï and G. Bertrand, *Chem. Rev.*, 2000, **100**, 39–92.
- G. Bertrand, *Carbene chemistry: from fleeting intermediates to powerful reagents*, Marcel Dekker, Inc., New York, 2002.
- K. Hirai, T. Itoh and H. Tomioka, *Chem. Rev.*, 2009, **109**, 3275–3332.
- P. de Frémont, N. Marion and S. P. Nolan, *Coord. Chem. Rev.*, 2009, **253**, 862–892.
- R. A. Moss and M. P. Doyle, *Contemporary Carbene Chemistry*, John Wiley & Sons, Hoboken, 2013.
- M. N. Hopkinson, C. Richter, M. Schedler and F. Glorius, *Nature*, 2014, **510**, 485–496.
- R. S. Sheridan, *Chem. Rev.*, 2013, **113**, 7179–7208.
- D. Gerbig and D. Ley, *WIREs Comput. Mol. Sci.*, 2013, **3**, 242–272.
- H. F. Schaefer, *Science*, 1986, **231**, 1100–1107.
- B. Luke, J. Pople, M. Krogh-Jespersen, Y. Apeloig, J. Chandrasekhar and P. v. R. Schleyer, *J. Am. Chem. Soc.*, 1986, **108**, 260–269.
- B. Luke, J. Pople, M. Krogh-Jespersen, Y. Apeloig, M. Karni, J. Chandrasekhar and P. v. R. Schleyer, *J. Am. Chem. Soc.*, 1986, **108**, 270–284.
- W. P. Neumann, *Chem. Rev.*, 1991, **91**, 311–334.
- C. Heinemann, W. A. Herrmann and W. Thiel, *J. Organomet. Chem.*, 1994, **475**, 73–84.
- M. Haaf, T. A. Schmedake and R. West, *Acc. Chem. Res.*, 2000, **33**, 704–714.
- Y. Mizuhata, T. Sasamori and N. Tokitoh, *Chem. Rev.*, 2009, **109**, 3479–3511.
- Y. Wang and J. Ma, *J. Organomet. Chem.*, 2009, **694**, 2567–2575.
- D. E. Falvey, *J. Phys. Org. Chem.*, 1999, **12**, 589–596.
- G. I. Borodkin and V. G. Shubin, *Russ. Chem. Rev.*, 2008, **77**, 395.
- H. Braunschweig, C.-W. Chiu, K. Radacki and T. Kupfer, *Angew. Chem. Int. Ed.*, 2010, **49**, 2041–2044.
- J. Hicks, P. Vasko, J. M. Goicoechea and S. Aldridge, *Nature*, 2018, **557**, 92.
- A. Hinz and F. Breher, *Angew. Chem. Int. Ed.*, 2018, **57**, 8818–8820.
- C. J. Cramer, F. J. Dulles, J. W. Storer and S. E. Worthington, *Chem. Phys. Letters*, 1994, **218**, 387–394.
- I. D. Hyatt, M. E. Meza-Aviña and M. P. Croatt, *Synlett*, 2012, **23**, 2869.
- V. Kunde, A. Aikin, R. Hanel, D. Jennings, W. Maguire and R. Samuelson, *Nature*, 1981, **292**, 686.
- V. Morris, S. Bhatia, A. Stelson and J. Hall Jr, *Energy & Fuels*, 1991, **5**, 126–133.
- J. S. Francisco, *Chem. Phys. Lett.*, 1994, **230**, 372–376.
- D. Wang, H. Liu, X. Huang, Y. Li, C. Geng, J. Zhan and C. Sun, *Eur. Phys. J. D*, 2008, **48**, 187–196.
- J. Adamson, J. DeSain, R. Curl and G. Glass, *J. Phys. Chem. A*, 1997, **101**, 864–870.
- Y. Osamura and S. Petrie, *J. Phys. Chem. A*, 2004, **108**, 3615–3622.
- H.-L. Chen and W.-C. Chao, *J. Phys. Chem. A*, 2011, **115**, 1133–1142.
- B. Turner, L. Pirogov and Y. Minh, *Astrophys. J.*, 1997, **483**, 235.
- P. Pratap, J. Dickens, R. L. Snell, M. Miralles, E. Bergin, W. M. Irvine and F. Schloerb, *Astrophys. J.*, 1997, **486**, 862.
- T. Hirota, S. Yamamoto, H. Mikami and M. Ohishi, *Astrophys. J.*, 1998, **503**, 717.
- H. Liszt and R. Lucas, *Astron. Astrophys.*, 2001, **370**, 576–585.
- A. Mebel and R. Kaiser, *Astrophys. J.*, 2002, **564**, 787.
- K. Takahashi and T. Takayanagi, *Chem. Phys. Letters*, 2006, **429**, 399–404.
- J.-C. Loison, V. Wakelam and K. M. Hickson, *Mon. Notices Royal Astron. Soc.*, 2014, **443**, 398–410.
- J. Loison and K. Hickson, *Chem. Phys. Lett.*, 2015, **635**, 174–179.

- 46 A. M. Shivani and P. T. Shivani, *Orig. Life Evol. Biospheres*, 2014, **44**, 143–157.
- 47 D. V. Lanzisera and L. Andrews, *J. Phys. Chem. A*, 1997, **101**, 9660–9665.
- 48 D. V. Lanzisera, L. Andrews and P. R. Taylor, *J. Phys. Chem. A*, 1997, **101**, 7134–7140.
- 49 J. M. Merritt, G. E. Doublerly, P. L. Stiles and R. E. Miller, *J. Phys. Chem. A*, 2007, **111**, 12304–12316.
- 50 T. Liang and G. E. Doublerly, *Chem. Phys. Lett.*, 2012, **551**, 54–59.
- 51 A. Pappova, C. A. Deakynoe, A. Skancke, I. Černušák and J. F. Liebman, *Mol. Phys.*, 1996, **89**, 247–265.
- 52 J. F. Liebman, I. Černušák and A. Miková, *Int. J. Quant. Chem*, 2001, **84**, 140–148.
- 53 R. Bernheim, R. Kempf, P. Humer and P. Skell, *J. Chem. Phys.*, 1964, **41**, 1156–1157.
- 54 R. Bernheim, R. Kempf, J. Gramas and P. Skell, *J. Chem. Phys.*, 1965, **43**, 196–200.
- 55 R. Bernheim, R. Kempf and E. Reichenbecher, *J. Magn. Reson.*, 1970, **3**, 5–9.
- 56 E. Wasserman, W. Yager and V. Kuck, *Chem. Phys. Lett.*, 1970, **7**, 409–413.
- 57 A. Dendramis and G. Leroi, *J. Chem. Phys.*, 1977, **66**, 4334–4340.
- 58 S. Saito, Y. Endo and E. Hirota, *J. Chem. Phys.*, 1984, **80**, 1427–1430.
- 59 P.-Å. Malmquist, R. Lindh, B. O. Roos and S. Ross, *Theor. Chim. Acta.*, 1988, **73**, 155–171.
- 60 F. Brown, S. Saito and S. Yamamoto, *J. Mol. Spect.*, 1990, **143**, 203–208.
- 61 Y. Endo and O. Yasuhiro, *J. Chem. Phys.*, 1993, **98**, 6618–6623.
- 62 C. Miller, W. Eckhoff and R. Curl, *J. Mol. Struct.*, 1995, **352**, 435–446.
- 63 M. McCarthy, C. Gottlieb, A. Cooksy and P. Thaddeus, *J. Chem. Phys.*, 1995, **103**, 7779–7787.
- 64 G. Maier, H. P. Reisenauer and K. Rademacher, *Chem.:Eur. J.*, 1998, **4**, 1957–1963.
- 65 F. Sun, A. Kosterev, G. Scott, V. Litosh and R. Curl, *J. Chem. Phys.*, 1998, **109**, 8851–8856.
- 66 J.-x. Han, P. Hung, J. DeSain, W. Jones and R. Curl, *J. Mol. Spect.*, 1999, **198**, 421–428.
- 67 M. D. Allen, K. M. Evenson and J. M. Brown, *J. Mol. Spect.*, 2001, **209**, 143–164.
- 68 P. Hung, F. Sun, N. Hunt, L. Burns and R. Curl, *J. Chem. Phys.*, 2001, **115**, 9331–9339.
- 69 J. C. Poutsma, S. D. Upshaw, R. R. Squires and P. G. Wenthold, *J. Phys. Chem. A*, 2002, **106**, 1067–1073.
- 70 M. R. Nimlos, G. Davico, C. M. Geise, P. G. Wenthold, W. C. Lineberger, S. J. Blanksby, C. M. Hadad, G. A. Petersson and G. B. Ellison, *J. Chem. Phys.*, 2002, **117**, 4323–4339.
- 71 M. Nakajima, H. Toyoshima, S. Sato, K. Tanaka, K. Hoshina, H. Kohguchi, Y. Sumiyoshi, Y. Ohshima and Y. Endo, *J. Chem. Phys.*, 2013, **138**, 164309.
- 72 G. A. Garcia, J. Krüger, B. Gans, C. Falvo, L. H. Coudert and J.-C. Loison, *J. Chem. Phys.*, 2017, **147**, 013908.
- 73 J. Harrison, A. Dendramis and G. Leroi, *J. Am. Chem. Soc.*, 1978, **100**, 4352–4356.
- 74 M. E. Zandler, J. D. Goddard and H. F. Schaefer, *J. Am. Chem. Soc.*, 1979, **101**, 1072–1076.
- 75 K. S. Kim, H. F. Schaefer, L. Radom, J. A. Pople and J. S. Binkley, *J. Am. Chem. Soc.*, 1983, **105**, 4148–4154.
- 76 J. E. Rice and H. F. Schaefer, *J. Chem. Phys.*, 1987, **86**, 7051–7053.
- 77 E. T. Seidl and H. F. Schaefer, *J. Chem. Phys.*, 1992, **96**, 4449–4452.
- 78 K. Aoki, H. Fueno, S. Ikuta and O. Nomura, *Chem. Phys. letters*, 1993, **202**, 33–36.
- 79 K. Aoki, S. Ikuta and O. Nomura, *J. Chem. Phys.*, 1993, **99**, 3809–3814.
- 80 C. B. Kellogg, J. M. Galbraith, J. E. Fowler and H. F. Schaefer, *J. Chem. Phys.*, 1994, **101**, 430–435.
- 81 C. Morter, S. Farhat and R. Curl, *Chem. Phys. letters*, 1993, **207**, 153–158.
- 82 N. Goldberg, A. Fiedler and H. Schwarz, *J. Phys. Chem.*, 1995, **99**, 15327–15334.
- 83 J. Koput, *J. Phys. Chem. A*, 2002, **106**, 6183–6188.
- 84 J. Koput, *J. Phys. Chem. A*, 2003, **107**, 4717–4723.
- 85 E. Ionescu and S. A. Reid, *J. Mol. Struct.: THEOCHEM*, 2005, **725**, 45–53.
- 86 M. Kassae, S. Musavi and F. Buazar, *J. Mol. Struct.: THEOCHEM*, 2005, **728**, 15–24.
- 87 M. Mladenović, P. Botschwina and C. Puzzarini, *J. Phys. Chem. A*, 2006, **110**, 5520–5529.
- 88 M. Kassae, M. Ghambarian and S. Musavi, *Heteroatom Chemistry*, 2008, **19**, 377–388.
- 89 Z.-X. Zhao, H.-X. Zhang and C.-C. Sun, *J. Phys. Chem. A*, 2008, **112**, 12125–12131.
- 90 N. Inostroza, X. Huang and T. J. Lee, *J. Chem. Phys.*, 2011, **135**, 244310.
- 91 J. Cernicharo, C. Gottlieb, M. Guélin, P. Thaddeus and J. Vrtilik, *Astrophys. J.*, 1989, **341**, L25–L28.
- 92 M. Guélin, S. Muller, J. Cernicharo, A. Apponi, M. McCarthy, C. Gottlieb and P. Thaddeus, *Astronomy and Astrophysics*, 2000, **363**, L9–L12.
- 93 M. Guélin, S. Muller, J. Cernicharo, M. McCarthy and P. Thaddeus, *Astronomy & Astrophysics*, 2004, **426**, L49–L52.
- 94 A. Apponi, M. McCarthy, C. Gottlieb and P. Thaddeus, *Astrophys. J. Lett.*, 1999, **516**, L103.
- 95 M. E. Sanz, M. C. McCarthy and P. Thaddeus, *Astrophys. J. Lett.*, 2002, **577**, L71.
- 96 Z.-X. Zhao, C.-Y. Hou, X. Shu, H.-X. Zhang and C.-c. Sun, *Theor. Chem. Acc.*, 2009, **124**, 85–93.
- 97 J. Flores, I. Perez-Juste and L. Carballeira, *Chem. Phys.*, 2005, **313**, 1–15.
- 98 Q. Wang, Y.-h. Ding and C.-c. Sun, *Chem. Phys.*, 2006, **323**, 413–428.

- 99 J. Kalcher, *J. Phys. Chem. A*, 2005, **109**, 11437–11442.
- 100 J. Kalcher, P. Skurski and J. Simons, *J. Phys. Chem. A*, 2007, **111**, 401–410.
- 101 S. Thorwirth and M. E. Harding, *J. Chem. Phys.*, 2009, **130**, 214303.
- 102 J.-i. Yamamoto and Y. Okabe, *Comput. Theor. Chem.*, 2011, **963**, 24–33.
- 103 M. Onyszczuk, A. Castel, P. Riviere and J. Satge, *J. Organomet. Chem.*, 1986, **317**, C35–C37.
- 104 G. Hihara, R. C. Hynes, A.-M. Lebuis, M. Rivière-Baudet, I. Wharf and M. Onyszczuk, *J. Organomet. Chem.*, 2000, **598**, 276–285.
- 105 Z. D. Brown, P. Vasko, J. C. Fettinger, H. M. Tuononen and P. P. Power, *J. Am. Chem. Soc.*, 2012, **134**, 4045–4048.
- 106 M. Huang and M.-D. Su, *J. Organomet. Chem.*, 2002, **659**, 121–124.
- 107 Q. Wang, Y.-h. Ding and C.-c. Sun, *J. Chem. Phys.*, 2005, **122**, 204305.
- 108 A. Bundhun, H. H. Abdallah, P. Ramasami, P. P. Gaspar and H. F. Schaefer, *Inorg. Chem.*, 2012, **51**, 12152–12164.
- 109 M. Kassaei, M. Ghambarian and S. Musavi, *J. Organomet. Chem.*, 2005, **690**, 4692–4703.
- 110 S. Xu and M. Lin, *J. Phys. Chem. A*, 2007, **111**, 6730–6740.
- 111 R.-C. Jian, C. Tsai, L.-C. Hsu and H.-L. Chen, *J. Phys. Chem. A*, 2010, **114**, 4655–4663.
- 112 H.-L. Chen, S.-k. Wu and Y.-H. Lu, *J. Phys. Chem. A*, 2012, **116**, 3267–3273.
- 113 N.-N. Wu, C.-Z. He, X.-M. Duan and J.-Y. Liu, *Journal of computational chemistry*, 2011, **32**, 1449–1455.
- 114 M. R. Berman, T. Tsuchiya, A. Gregušová, S. A. Perera and R. J. Bartlett, *J. Phys. Chem. A*, 2007, **111**, 6894–6899.
- 115 C. Pizzarini and A. Gambi, *J. Chem. Phys.*, 2005, **122**, 064316.
- 116 P. Antoniotti, S. Borocci, N. Bronzolino and F. Grandinetti, *ChemPhysChem*, 2004, **5**, 1345–1351.
- 117 S. A. Betterton, A. S. Berka and P. E. Fleming, *J. Theor. Comput. Chem.*, 2010, **9**, 189–200.
- 118 J. Staton, *Chem. Phys. Lett.*, 1997, **281**, 130–134.
- 119 R. J. Bartlett, J. D. Watts, S. Kucharski and J. Noga, *Chem. Phys. Lett.*, 1990, **165**, 513–522.
- 120 K. Raghavachari, G. W. Trucks, J. A. Pople and M. Head-Gordon, *Chem. Phys. Lett.*, 2013, **589**, 37–40.
- 121 R. A. Kendall, T. H. Dunning and R. J. Harrison, *J. Chem. Phys.*, 1992, **96**, 6796–6806.
- 122 T. H. Dunning Jr, *J. Chem. Phys.*, 1989, **90**, 1007–1023.
- 123 D. E. Woon and T. H. Dunning Jr, *J. Chem. Phys.*, 1993, **98**, 1358–1371.
- 124 T. H. Dunning Jr, K. A. Peterson and A. K. Wilson, *J. Chem. Phys.*, 2001, **114**, 9244–9253.
- 125 N. J. DeYonker, K. A. Peterson and A. K. Wilson, *J. Phys. Chem. A*, 2007, **111**, 11383–11393.
- 126 A. K. Wilson, D. E. Woon, K. A. Peterson and T. H. Dunning Jr, *J. Chem. Phys.*, 1999, **110**, 7667–7676.
- 127 J. F. Stanton, J. Gauss, L. Cheng, M. E. Harding, D. A. Matthews and P. G. Szalay, *CFOUR, Coupled-Cluster techniques for Computational Chemistry, a quantum-chemical program package*, With contributions from A.A. Auer, R.J. Bartlett, U. Benedikt, C. Berger, D.E. Bernholdt, Y.J. Bomble, O. Christiansen, F. Engel, R. Faber, M. Heckert, O. Heun, M. Hilgenberg, C. Huber, T.-C. Jagau, D. Jonsson, J. Jusélius, T. Kirsch, K. Klein, W.J. Lauderdale, F. Lipparini, T. Metzroth, L.A. Mück, D.P. O'Neill, D.R. Price, E. Prochnow, C. Puzzarini, K. Ruud, F. Schiffmann, W. Schwalbach, C. Simmons, S. Stopkowitz, A. Tajti, J. Vázquez, F. Wang, J.D. Watts and the integral packages MOLECULE (J. Almlöf and P.R. Taylor), PROPS (P.R. Taylor), ABACUS (T. Helgaker, H.J. Aa. Jensen, P. Jørgensen, and J. Olsen), and ECP routines by A. V. Mitin and C. van Wüllen. For the current version, see <http://www.cfour.de>.
- 128 H.-J. Werner, P. J. Knowles, G. Knizia, F. R. Manby and M. Schütz, *WIREs Comput. Mol. Sci.*, 2012, **2**, 242–253.
- 129 H.-J. Werner, P. J. Knowles, G. Knizia, F. R. Manby, M. Schütz, P. Celani, W. Györfy, D. Kats, T. Korona, R. Lindh, A. Mitrushenkov, G. Rauhut, K. R. Shamasundar, T. B. Adler, R. D. Amos, A. Bernhardsson, A. Berning, D. L. Cooper, M. J. O. Deegan, A. J. Dobbyn, F. Eckert, E. Goll, C. Hampel, A. Hesselmann, G. Hetzer, T. Hrenar, G. Jansen, C. Köppl, Y. Liu, A. W. Lloyd, R. A. Mata, A. J. May, S. J. McNicholas, W. Meyer, M. E. Mura, A. Nicklass, D. P. O'Neill, P. Palmieri, D. Peng, K. Pflüger, R. Pitzer, M. Reiher, T. Shiozaki, H. Stoll, A. J. Stone, R. Tarroni, T. Thorsteinsson and M. Wang, *MOLPRO, version 2015.1, a package of ab initio programs*, 2015, see <http://www.molpro.net>.
- 130 M. S. Schuurman, S. R. Muir, W. D. Allen and H. F. Schaefer, *J. Chem. Phys.*, 2004, **120**, 11586–11599.
- 131 J. M. Gonzales, C. Pak, R. S. Cox, W. D. Allen, H. F. Schaefer, A. G. Császár and G. Tarczay, *Chem. Eur. J.*, 2003, **9**, 2173–2192.
- 132 A. G. Császár, W. D. Allen and H. F. Schaefer, *J. Chem. Phys.*, 1998, **108**, 9751–9764.
- 133 A. L. L. East and W. D. Allen, *J. Chem. Phys.*, 1993, **99**, 4638–4650.
- 134 M. E. Harding, T. Metzroth, J. Gauss and A. A. Auer, *Journal of Chemical Theory and Computation*, 2008, **4**, 64–74.
- 135 *MRCC, a quantum chemical program suite written by M. Kállay, Z. Rolik, J. Csontos, P. Nagy, G. Samu, D. Mester, J. Csóka, B. Szabó, I. Ladjánszki, L. Szegedy, B. Ladóczki, K. Petrov, M. Farkas, P. D. Mezei, and B. Hégyel. www.mrcc.hu*.
- 136 M. Kállay and J. Gauss, *J. Chem. Phys.*, 2008, **129**, 144101.
- 137 D. Feller, K. A. Peterson and T. D. Crawford, *J. Chem. Phys.*, 2006, **124**, 054107.
- 138 T. Helgaker, W. Klopper, H. Koch and J. Noga, *J. Chem. Phys.*, 1997, **106**, 9639–9646.
- 139 Z. Rolik, L. Szegedy, I. Ladjánszki, B. Ladóczki and M. Kállay, *J. Chem. Phys.*, 2013, **139**, 094105.
- 140 D. E. Woon and T. H. Dunning Jr, *J. Chem. Phys.*, 1995, **103**, 4572–4585.
- 141 K. A. Peterson and T. H. Dunning Jr, *J. Chem. Phys.*, 2002,

- 117, 10548–10560.
- 142 L. Cheng and J. Gauss, *J. Chem. Phys.*, 2011, **135**, 084114.
- 143 E. D. Glendening, C. R. Landis and F. Weinhold, *WIREs Comput. Mol. Sci.*, 2012, **2**, 1–42.
- 144 Shao, Y.; Gan, Z.; Epifanovsky, E.; Gilbert, A. TB; Wormit, M.; Kussmann, J.; Lange, A. W.; Behn, A.; Deng, J.; Feng, X. et al., *Mol. Phys.*, 2015, **113**, 184–215.
- 145 C. Lee, W. Yang and R. G. Parr, *Physical review B*, 1988, **37**, 785.
- 146 *CYLview, 1.0b*, Legault, C. Y., Université de Sherbrooke, 2009 (<http://www.cylview.org>).
- 147 P. Pyykkö, *Annu. Rev. Phys. Chem.*, 2012, **63**, 45–64.
- 148 W. J. Hehre, R. Ditchfield, L. Radom and J. A. Pople, *J. Am. Chem. Soc.*, 1970, **92**, 4796–4801.
- 149 A. K. Eckhardt and P. R. Schreiner, *Angew. Chem. Int. Ed.*, 2018, **57**, 5248–5252.

The lowest lying singlet and triplet states of nine relatives of cyanomethylene are studied with highly rigorous *ab initio* methods, and periodic trends in their electronic structures are analyzed.

